



OPEN

SUBJECT AREAS:
NANOSCIENCE AND
TECHNOLOGY
MATERIALS SCIENCEReceived
5 September 2013Accepted
29 January 2014Published
18 February 2014Correspondence and
requests for materials
should be addressed to
C.-G.D. (wxbcdcg@
gmail.com) or Y.W.L.
(yaowen@tongji.edu.
cn)

Picosecond electric field pulse induced coherent magnetic switching in MgO/FePt/Pt(001)-based tunnel junctions: a multiscale study

Wanjiao Zhu¹, Dun Xiao², Yaowen Liu², S. J. Gong¹ & Chun-Gang Duan^{1,3}

¹Key Laboratory of Polar Materials and Devices, Ministry of Education, East China Normal University, Shanghai 200241, China, ²Shanghai Key Laboratory of Special Artificial Microstructure Materials and Technology, School of Physical Science and Engineering, Tongji University, Shanghai 200092, China, ³National Laboratory for Infrared Physics, Chinese Academy of Sciences, Shanghai 200083, China.

Combined methods of first-principles calculations and Landau-Lifshitz-Gilbert (LLG) macrospin simulations are performed to investigate the coherent magnetization switching in the MgO/FePt/Pt(001)-based magnetic tunnel junctions triggered by short pulses of electric field through the control of magnetic anisotropy energy (MAE) electrically. First-principles calculations indicate that the MAE of MgO/FePt/Pt(001) film varies linearly with the change of the electric field, whereas the LLG simulations show that the change in MAE by electric field pulses could induce the in-plane magnetization reversal of the free layer by tuning the pulse parameters. We find that there exist a critical pulse width τ_{\min} to switch the in-plane magnetization, and this τ_{\min} deceases with the increasing pulse amplitude E_0 . Besides, the magnetization orientation cannot be switched when the pulse width exceeds a critical value τ_{\max} , and τ_{\max} increases asymptotically with E_0 . In addition, there exist some irregular switching areas at short pulse width due to the high precessional frequency under small initial angle. Finally, a successive magnetization switching can be achieved by a series of electric field pulses.

Spintronics has played a significant role in the development of magnetic data storage devices such as the nonvolatile magnetic random access memories (MRAM)^{1,2}. Traditional methods to control the magnetization generally require external magnetic field, which is inconvenient when the magnetic cells reach nanometer size. In the past decades, considerable interest has been stimulated to investigate the spin transfer torque (STT) effect^{3,4}, which utilizes the spin current to switch magnetization in nanopillars with perpendicular magnetic anisotropy⁵⁻⁸. This strategy can overcome the limit of length/width aspect ratio in the magnetic elements with in-plane magnetization and greatly improve the data storage area density. However, it has brought some problems in energy consumption. The critical switching current in this kind of magnetic tunnel junction (MTJ) or spin valve has the magnitude of 10^7 A/cm² or even higher⁹⁻¹¹. Such high current density even could bring physical damages to the devices. Therefore, it would be of great importance to find a new stimulus to manipulate the magnetization orientation.

Magnetization control by means of electric field is such a promising strategy to lower the energy consumption. In order to achieve this aim, the search for fundamental and practical solution to modulate the surface/interface magnetism by electric fields is a vital issue. Currently there exist two ways to control magnetization by electric field. One is to explore the heterostructures with ferroelectric and ferromagnetic constituents¹²⁻¹⁵. In these structures an applied electric field can influence the magnetic properties of ferromagnetic compounds by either inducing a strain in ferroelectric layers, which can be transferred into ferromagnetic compounds through the magnetostrictive coupling^{16,17}, or switching the ferroelectric polarization, which affects the interfacial magnetism through interfacial magnetoelectric (ME) effect^{12,18,19}. Another approach is accomplishing the direct control of magnetism in ferromagnetic metal by an electric field²⁰⁻²², which is triggered by spin-dependent screening²³. Nowadays, with the development of the computer capability and the material epitaxial growth technology, many reports have demonstrated that the applied electric fields through the above two approaches can effectively manipulate the magnetic properties of the surface/interface and nanostructure, including the electric control



of surface/interface magnetization^{12,19,21,24–27}, magnetic order^{28–30}, exchange bias^{31,32}, Rashba spin-orbit effect^{33,34} and magnetic anisotropy energy (MAE)^{13,20–22,35,36}. Among these properties, the MAE, which determines the stable magnetization direction, has attracted much more attention due to its crucial role in the study of data storage devices with low power consumption. In experiment, up to 4.5%(1%) coercivity change of FePt(Pd) films was observed with the applied voltage when immersed in a liquid electrolyte²⁰. Also the magnetic easy axis was manipulated in the dilute magnetic semiconductor (Ga,Mn)As³⁵. Recently, theoretical reports indicate that the external electric field can induce a linear change in surface MAE of typical ferromagnetic metals²¹, such as Fe, Co, and related materials³⁷, which have been proved experimentally³⁶.

Meanwhile, it is shown that an electric field alone cannot break time-reversal symmetry, so an assistant small magnetic field is required when considering the electric field induced magnetization switching. Both experimental and theoretical works have proved that the applied electric field can successfully change the magnetization orientation in MTJs^{38,39}. It is demonstrated that in CoFeB/MgO/CoFeB MTJ applied voltage can reduce the coercivity of the free CoFeB layer obviously, so it only needs a small spin current ($\sim 10^4$ A/cm²) to switch the magnetization⁴⁰. Also in FeCo/MgO/Fe MTJ, Y. Shiota *et al.*⁴¹ have designed a new method that electric field pulses can change the magnetic anisotropy of FeCo and induce a coherent precessional magnetization switching between two stable states. After that, by inducing a change of the magnetic easy axis of a very thin CoFeB film under the effect of electric field pulse, S. Kanai *et al.*⁴² have observed the switching of perpendicular component of magnetization in CoFeB/MgO MTJ. Besides, through adding a charge-trapping layer in the heterostructure, like Ag/Fe/MgO/ZrO₂, it can provide non-volatility to ME effect and develop some related memory devices⁴³. Based on these accomplishments, it is predicted that tuning the magnetic anisotropy by electric fields would open up a new prospect for the future applications in magnetic data storage.

To have a deeper understanding on the field control of MAE and the dynamics of magnetization switching in the magnetic nanostructures, we adopt a multiscale calculation method⁴⁴ that combines first-principles total energy calculations and macrospin simulations in present study. This method consists two major steps: firstly, first-principles total energy calculations are performed to gain the electric field dependence of the MAE of the multilayer system; then, the macrospin model based on the Landau-Lifshitz-Gilbert (LLG) equation is employed to simulate the coherent magnetization switching triggered by pulses of electric fields. Finally, by varying the amplitude and width of the electric field pulse, we could obtain a clear picture to show how the applied electric field pulses manipulate the magnetization orientation.

Results

The MgO/FePt/Pt(001) film is chosen as a candidate for the first-principles calculations. The structure is shown in the inset of Figure 1. Here the L1₀ ordered FePt layer makes main contribution in the MAE of the whole system. It has confirmed that the L1₀ ordered FePt thin film has a very high perpendicular magnetic anisotropy, about 1.1 meV/f. u.⁴⁵, and has been considered as a good candidate for the ultrahigh density recording media.

We calculate the MAE for first-principles calculation based on density functional theory (see Methods for details). Figure 1 shows the dependence of MAE on the external electric field magnitude. Note that the applied electric field is reduced by a factor when being across the MgO layer, which equals to the high frequency dielectric constant ϵ_{∞} of MgO⁴⁶. Thus it is necessary to convert the electric field amplitude in vacuum to the actual amplitude across the MgO layer by dividing the $\epsilon_{\infty} \approx 3$. All the following discussions about the electric field amplitude also consider the field in MgO. Without the applied

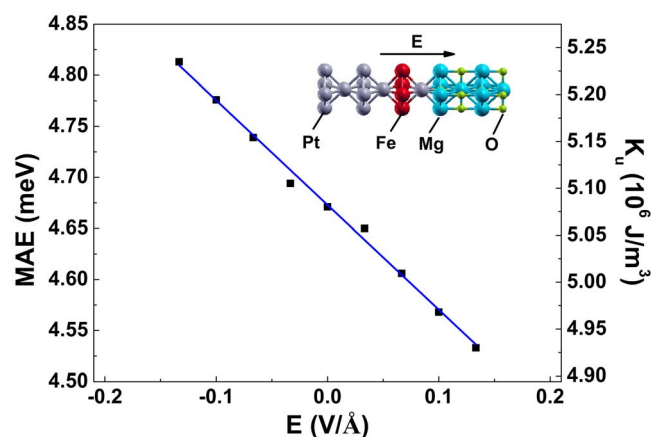


Figure 1 | Magnetic anisotropy energy (MAE) and corresponding magnetic anisotropy density K_u of MgO/FePt/Pt(001) film as a function of applied electric field in the MgO layer. The solid blue line is a linear fit to the calculated data. The inset shows the structure model of MgO/FePt/Pt(001) film and the negative direction of electric field is indicated by the black arrow.

electric field (i.e. $E = 0$), the calculated MAE of the system is about 4.6 meV. This value agrees well with previous theoretical works³⁷. It can be seen clearly that within the calculation accuracy the MAE changes linearly with the electric field from -0.13 to 0.13 V/Å. The MAE coefficient β_S is defined as $\beta_S = \Delta K_u/E$, where ΔK_u is the change of K_u , whose value is displayed at the right y-axis of Figure 1. From the slope rate of the figure, we get $\beta_S \approx 111.6$ μ J/V m². Comparing the result with that for the Fe(001) surface ($\beta_S \approx 9.5$ μ J/V m²)²¹, the ME coupling in the MgO/FePt/Pt system is very remarkable, indicating that the MAE can be manipulated in a broad range by applying electric field. By analyzing the electron band structure, the present study indicates that the linear ME coupling effect is mainly caused by the electric field induced modification of the relative minority electron occupation in Fe 3d orbitals, especially the d_{xy} and $d_{xz(yz)}$, which lead to the change of orbital momentum therefore the spin-orbit coupling of electrons at the surface of the conducting magnetic layers^{21,46}.

In order to gain insight into how the magnetization dynamically respond to the stimulus of the electric field in a full MgO-based MTJ structure, simulations based on the LLG equation have been performed. The structure model is shown in Figure 2a, in which the free layer has the structure of FePt/Pt(001) with the perpendicular easy axis and the fixed layer is magnetized in the film-plane along y axis direction. Here we consider the junction pillar to have an ellipse in-plane dimension. Thus the stable state of the in-plane component of magnetization vector in free layer is along the y axis direction, i.e., the long axis of the ellipse, because of the shape anisotropy. All the details for the simulation can be seen in Methods section.

The mechanism of the electric field pulse induced magnetization switching is illustrated in Figure 2c. Without the electric field pulse, summarizing all the other contributions lead to the effective field H_{eff} in the y - z plane with a tilt angle of 60° with respect to the z axis, so that the initial equilibrium state of magnetization is along this effective field H_{eff} direction (see Figure 2c). When the negative electric field is applied, the H_{eff} will change its direction since the electric field contributes an additional surface perpendicular MAE, which drives the easy axis of the effective field closer to the z direction. Consequently, the magnetization then starts to precess around the new easy axis with a tendency to align with the new effective field, as illustrated in Figure 2c. When the electric field pulse is switched off, the restructured effective field has two possible orientations: either in the left (brown line) or in the right (blue line) of z axis, which strongly depends on the pulse width as well as the transient orientation of

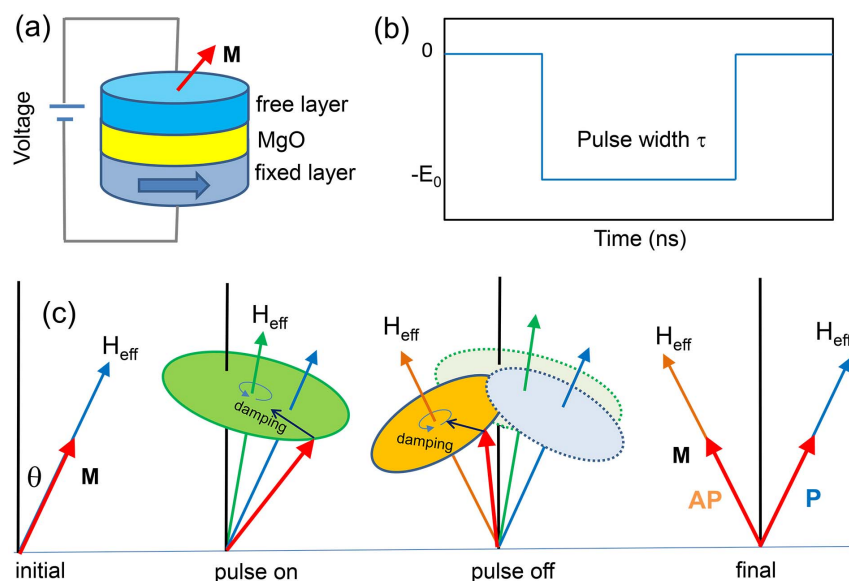


Figure 2 | (a) Illustration of the typical structure of magnetic tunnel junctions for the LLG simulation. Here the red arrow in the free and the blue arrow in fixed layer represent the respective magnetizations. (b) Shape of the applied electric field pulse used in the simulation. E_0 and τ are the amplitude and time width of the pulse, respectively. (c) Illustration of magnetization switching induced by the electric field. Here the green arrow represents the new effective field H_{eff} under the electric field pulse, and the brown and blue arrows are the possible orientation of H_{eff} with the pulse off.

the in-plane anisotropy field. As a result, the damped oscillation drives the magnetization to its final state in parallel or antiparallel alignment with respect to the magnetization of the fixed layer.

Two typical switching processes, *i.e.*, parallel (P) and antiparallel (AP), are respectively shown in Figure 3a and b, which monitor the evolution of the y -component of the magnetization (m_y). The simulations start from an equilibrium state at a tilt angle of 60° with the z axis. The initial m_y is parallel to the magnetization direction of the fixed layer. Then at the time of 3 ns, we apply a single, unipolar, rectangular-shaped electric field pulse with amplitude $E_0 = 0.04$ V/Å and pulse width τ . As expected, when the electric field induced perpendicular anisotropy is switched on (labeled as “Pulse start”), m_y exhibits a large angle oscillation due to an increase of perpendicular K_u . Here the modification of K_u by the external electric field is obtained from the first-principles calculations. As is clear from Figure 3, different τ corresponds to different final state. To be specific, when $\tau = 35, 80$ and 180 ps, the final magnetization m_y is parallel to the magnetization direction of the fixed layer, whereas for $\tau = 20, 55, 140, 230$ ps, the final m_y is at antiparallel position, *i.e.* the in-plane magnetization of the free layer is reversed after the application of external electric field pulse. As a comparison, the effect of constant external electric field (infinite τ) is shown as black solid lines in both Figure 3a and 3b. The final in-plane magnetization under the influence of constant electric field is a small but finite value determined by the strength of the electric field, as shown in the dash line in Figure 3a and 3b.

In order to explore the dominating factors to control the final state, we repeat the simulations with different pulse τ from 1 to 400 ps with 1 ps step. The results are summarized also in Figure 3. To make the results more explicit, those τ which could result in the magnetization reversal (AP) are shown as shaded plot. As a consequence, the plot is divided by blank (P) and shaded (AP) zones alternately. As is clear from the figure, only electric field pulse with appropriate time width τ could result in magnetization reversal. This finding brings two immediate conclusions: first, there exists a minimal time width τ_{min} of the field pulse, only when $\tau > \tau_{min}$ it is possible to reverse the magnetization; second, there also exists a maximal time width τ_{max} of the field pulse. If the pulse width is beyond τ_{max} , the electric field pulse will always drive m_y back to the P state and cannot trigger the

magnetization reversal to AP state. From the results in Figure 3a and 3b, It is found that the sign of m_y at the pulse ending time is not necessarily the final sign of m_y due to the large angle oscillation after the end of the applied pulse. From equation (1) in the Methods section, the LLG equation shows that the state of m in the next time is not only decided by its current position but also influenced by its variation with time t , *i.e.*, the term dm/dt . Thus it is significant to consider the “velocity” of the magnetization m when studying its final state.

The existence of τ_{max} can be explained by comparing the simulations under the constant electric field (the black curve in Figure 3a and 3b) and with those under electric field pulse. It is obvious that the oscillation amplitude of m_y decreases with the time because the new H_{eff} direction tends to be closer to the z axis due to the increased perpendicular MAE. If the pulse duration time exceeds τ_{max} , m_y will oscillates in a small range near the final average value, see the dash line in Figure 3a and 3b. This indicates that m_y will be trapped in P state and have no chance to enter AP state when the electric field vanishes. Thus it is important to tune the pulse width to realize the magnetization switching to AP state.

We have further studied the influence of amplitude of electric field pulse on magnetization switching. Figure 3c shows the critical minimal pulse width τ_{min} to trigger the switching and the maximal pulse width τ_{max} as a function with the pulse amplitude E_0 , respectively. Note that τ_{min} decreases with the enhancement of E_0 while τ_{max} increases. The main reason for behavior of τ_{min} is that with the increase of the pulse amplitude, there is a greater increase in value of K_u and perpendicular magnetic anisotropy field H_k . According to equation (1) in Methods section, this enhanced effect directly improves the rotation speed of magnetization along the z axis and thus τ_{min} reduces. For τ_{max} , the enhanced E_0 will increase both the amplitude and frequency of the m_y oscillation during the electric field pulse. This change can induce more switching time zone and therefore larger τ_{max} . These results imply that we can effectively accomplish the magnetization switching and cut down the necessary power consumption by applying the electric field pulse.

Furthermore, in order to obtain a clear picture about the influence of pulse width and amplitude on switching, we have simulated the P-to-AP switching under single pulses with different width and

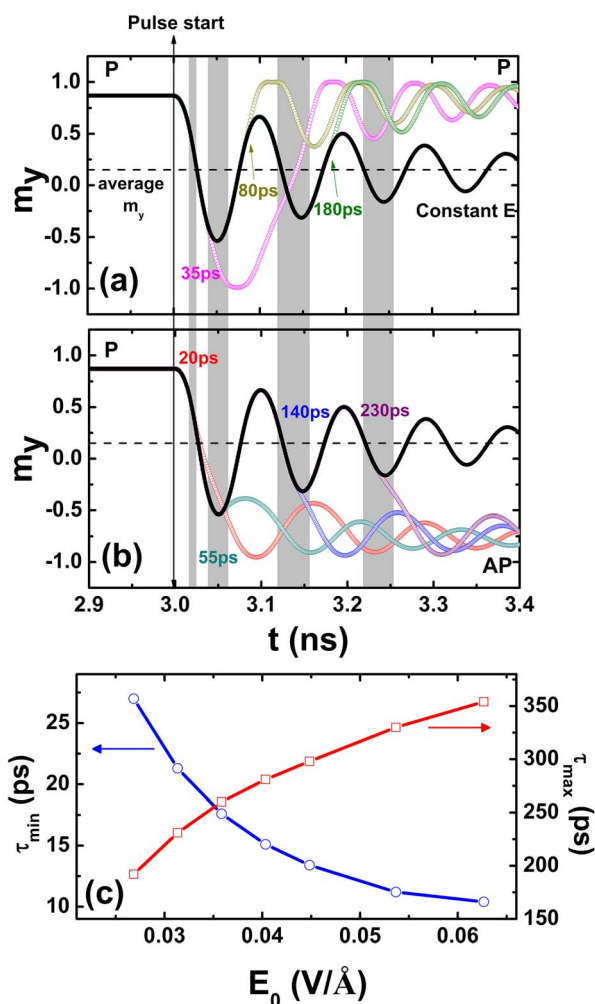


Figure 3 | (a) and (b) Temporal process of magnetization switching driven by a single electric field pulse with different time widths. The initial state is in the parallel state ($m_y > 0$), and the electric field pulse begins at $t = 3$ ns. The final state switches to AP state for $\tau = 20, 55, 140$ and 230 ps [see the color curves in (b)] and returns to P state for $\tau = 35, 80$ and 180 ps [see the color curves in (a)]. The black curve shows the magnetization precession under the constant electric field, instead of electric field pulses. The black dash line indicates the final average value of m_y under the constant electric field. The gray shadow area represents the P-AP switching time zone when the electric field pulse ends. (c) Dependence of the critical minimal pulse width τ_{\min} and maximal pulse width τ_{\max} on the pulse amplitude E_0 .

amplitude. Figure 4a & 4b summarize the switching probability as function of pulse width and amplitude, where yellow (blue) area denotes switching AP state (no switching, P state). From Figure 4a, for a given E_0 , it can be seen clearly that AP and P states happen alternatively with the increasing τ , and also number of switching area increases under a high E_0 , which all keep consistent with the results in Figure 3. More importantly, for a short pulse width, there exist some irregular switching regions, which indicate that we cannot control the switching effectively in the short τ ranges. One possible reason for this is that the small initial precessional angle θ with the z axis would bring a high perpendicular component of \mathbf{H}_{eff} , and this behavior would directly increase the Larmor frequency $f = \gamma/2\pi\mu_0 H_z$, where γ , μ_0 and H_z are the gyromagnetic constant, permeability in vacuum and the z component of \mathbf{H}_{eff} , and then drive the magnetization precesses fast along the z axis during the pulse. In order to clarify the origin of this irregular behavior, we just consider the enhanced in-plane shape anisotropy field \mathbf{H}_{in} and increase θ from 60.5° to 83.7° .

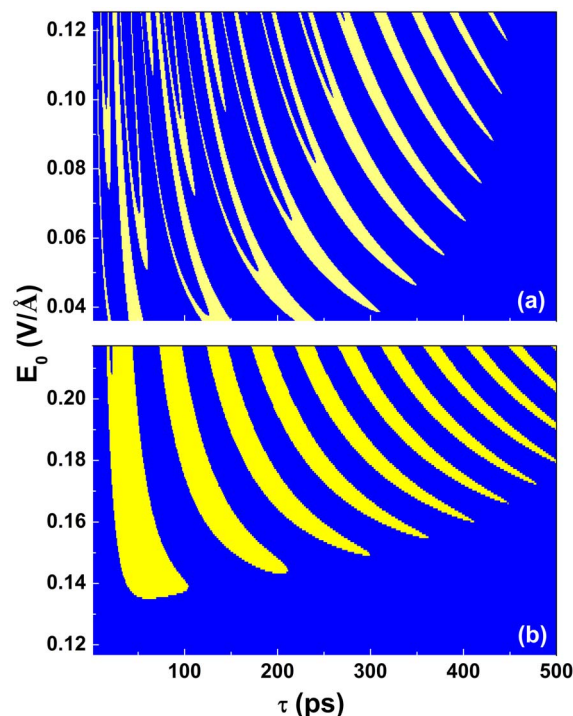


Figure 4 | P-to-AP Switching probability as function of the pulse width τ and amplitude E_0 for different initial precessional angle θ of magnetization with the $+z$ direction. (a) $\theta = 60.5^\circ$; (b) $\theta = 83.7^\circ$. Yellow and blue region represents the switching (AP state) and no switching (P state), respectively.

The results for this simulation are shown in Figure 4b. It is obvious that the switching regions become regular in the range of short pulse width, assuming that the large θ can induce a decrease in the precession frequency and keep the magnetization switching stable in a short time range during the pulse. Also it is noticed that the necessary pulse amplitude to trigger the switching is enhanced for a large θ because it needs more increase in K_u and perpendicular magnetic anisotropy field induced by electric field to let the \mathbf{H}_{eff} close to the z axis at the begin of switching. Therefore, we assume that it is significant to adjust the appropriate initial angle to control the pulse width and amplitude for the magnetization switching.

Finally, we have simulated the switching process induced by multiple pulses. Figure 5a displays the applied electric field pulses in the time duration of 27 ns. Each pulse has an interval time of 4 ns and keeps the same amplitude $E_0 = 0.04$ V/Å and time width $\tau = 50$ ps, shown in the inset zoom-in plot. From Figure 5b, we find that back and forth magnetization switching can be achieved with the picosecond multiple electric field pulses with the same polarity. Note that there exists a slightly small asymmetry in absolute value of m_y along the two different directions. The reason for this is mainly due to the influence of the applied external magnetic field, which has an orientation at a small tilt angle ($\sim 10^\circ$) from the z direction and favors the magnetization along the $+y$ direction. This shows unambiguously that we can repeatedly control the magnetization by appropriate electric field pulses.

Discussion

In summary, we have established a linear relationship between the MAE and the external electric field and achieved the magnetization switching induced by electric field pulse in the MgO/FePt/Pt(001)-based tunnel junctions through a combined strategy of first-principles and macrospin simulations. It is shown that back and forth switching can be realized with picosecond electric field pulses of the same polarity. The final magnetization state depends on pulse

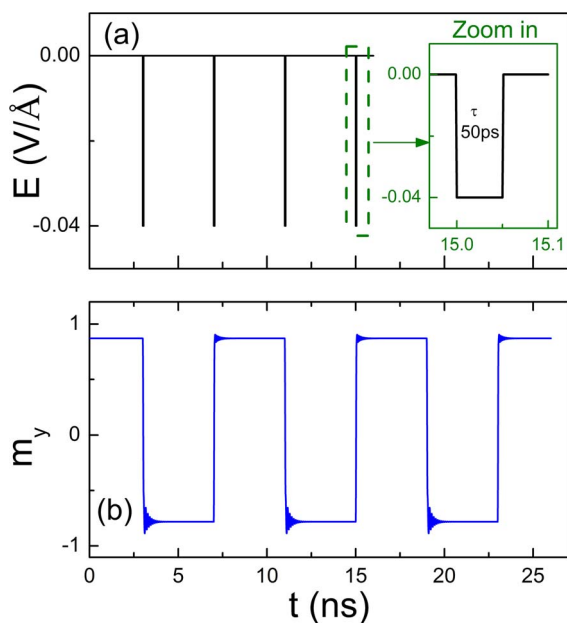


Figure 5 | The in-plane magnetization switching by multiple pulse. (a) The applied pulses during the switching. The inset zooms into the pulse at the time of 15 ns with the amplitude $E_0 = 0.04 \text{ V/Å}$ and width $\tau = 50 \text{ ps}$. Other pulses keep same in amplitude and width. (b) The magnetization switching between P and AP states. The beginning state is the P state.

width τ and there exist two critical pulse width values: the minimal pulse width τ_{\min} to trigger the switching and the maximal pulse width τ_{\max} . The minimal pulse width τ_{\min} decreases with the increasing pulse amplitude E_0 while τ_{\max} displays the opposite behavior. Meanwhile, by simulating the switching probability as function of pulse width and amplitude, we find some irregular switching regions in the situation of short pulse width, which is mainly because the small initial precessional angle leads to a high Larmor frequency and makes the magnetization decay to z direction fast during the pulse. Besides, it is demonstrated that a successive switching between P and AP states happens under the effect of multiple pulses. We expect these results to be helpful to develop the related devices in further experimental works.

Methods

In calculation of MAE we carry out density-functional calculations by using the projected augmented wave (PAW) method and treating the exchange correlation in the generalized gradient approximation (GGA), as implemented in Vienna Ab-initio Simulation Package (VASP)⁴⁷. We use the energy cut-off of 500 eV for the plane wave expansion and a $10 \times 10 \times 1$ Monkhorst-Pack grid for k -point mesh in the self-consistent calculations. The electric field here is introduced by the planar dipole layer method⁴⁸, and the negative electric field is defined as pointing from FePt to MgO layer at the FePt/MgO interface. To achieve the structural optimization, all the atoms are relaxed until their Hellman-Feynman forces are smaller than 2 meV/Å. The MAE is calculated by considering the difference between the total energies with the magnetization along the [100] and [001] orientations⁴⁹, in which the spin-orbital coupling is included. The magnetic anisotropy constant K_u is defined to be MAE per volume.

Because MAE has a tiny value compared with other energy of the film system, it is necessary to keep the high accuracy in the calculation. In our test calculation it is found that a good convergence of MAE has been accomplished at a 500 eV plane wave expansion cut-off energy and $40 \times 40 \times 1$ k -point mesh. Test calculation also shows that numbers of MgO and Pt layer have slight influence on the MAE, so during this part of work, in order to reduce the computational stress, the calculated model is set to containing 2 unit cells MgO and 4 layers Pt [see the inset of Figure 1].

In the simulation work, we integrate the LLG equation on a single domain, macrospin model. The simulation code is developed in-house and has been used in our previous study⁵⁰. This code now has been extended to consider the perpendicular surface MAE effect induced by the electric field pulses. This effect of the electric field induced magnetization dynamics of the free layer is modeled by including a change of perpendicular anisotropy into the LLG equation

$$\frac{dm}{dt} = -\gamma m \times H_{\text{eff}} + \alpha m \times \frac{dm}{dt} \quad (1)$$

where $m = M/M_s$ is the normalized magnetization of the free layer, α is the Gilbert damping factor, and γ is the gyromagnetic ratio. H_{eff} is the effective field containing a tilted magnetic anisotropy field, demagnetization field H_d and the external magnetic field H_{ex} . The perpendicular and in-plane components of the tilted anisotropy field are denoted by H_k and H_m , respectively. The electric field pulse induced surface MAE effect is introduced as a transient increment into the perpendicular anisotropy H_k . In this study, the external field $H_{\text{ex}} = 50 \text{ mT}$ is applied at a tilt angle of 10° from the film normal z direction. The typical parameters of FePt are chosen: $\mu_0 M_s = 1.43 \text{ T}$ (saturation magnetization), $K_u = 5.08 \times 10^6 \text{ J/m}^3$. The magnetization of the reference layer is fixed along the $+y$ direction. The thermal effect is ignored in this study.

- Chappert, C., Fert, A. & Van Dau, F. N. The emergence of spin electronics in data storage. *Nat. Mater.* **6**, 813–823 (2007).
- Bader, S. D. Colloquium: Opportunities in nanomagnetism. *Rev. Mod. Phys.* **78**, 1–15 (2006).
- Slonczewski, J. C. Current-driven excitation of magnetic multilayers. *J. Magn. Magn. Mater.* **159**, L1–L7 (1996).
- Berger, L. Emission of spin waves by a magnetic multilayer traversed by a current. *Phys. Rev. B* **54**, 9353 (1996).
- Mangin, S. *et al.* Current-induced magnetization reversal in nanopillars with perpendicular anisotropy. *Nat. Mater.* **5**, 210–215 (2006).
- Zhang, Z., Qiu, Y., Jin, Q. Y. & Liu, Y. Micromagnetic study of fieldlike spin torque effect on the magnetization switching in tunnel junctions with perpendicular anisotropy. *Appl. Phys. Lett.* **97**, 172501 (2010).
- Ravelosona, D. *et al.* Domain Wall Creation in Nanostructures Driven by a Spin-Polarized Current. *Phys. Rev. Lett.* **96**, 186604 (2006).
- Zeng, Z. *et al.* High-Power Coherent Microwave Emission from Magnetic Tunnel Junction Nano-oscillators with Perpendicular Anisotropy. *ACS Nano* **6**, 6115–6121 (2012).
- Seki, T., Mitani, S., Yakushiji, K. & Takanashi, K. Spin-polarized current-induced magnetization reversal in perpendicularly magnetized L1_0 -FePt layers. *Appl. Phys. Lett.* **88**, 172504 (2006).
- Meng, H. & Wang, J.-P. Spin transfer in nanomagnetic devices with perpendicular anisotropy. *Appl. Phys. Lett.* **88**, 172506 (2006).
- Nakayama, M. *et al.* Spin transfer switching in TbCoFe/CoFeB/MgO/CoFeB/TbCoFe magnetic tunnel junctions with perpendicular magnetic anisotropy. *J. Appl. Phys.* **103**, 07A710 (2008).
- Duan, C.-G., Jaswal, S. S. & Tsymbal, E. Y. Predicted Magnetoelectric Effect in Fe/BaTiO₃ Multilayers: Ferroelectric Control of Magnetism. *Phys. Rev. Lett.* **97**, 047201 (2006).
- Duan, C.-G., *et al.* Tailoring magnetic anisotropy at the ferromagnetic/ferroelectric interface. *Appl. Phys. Lett.* **92**, 122905 (2008).
- Gao, X. *et al.* Microstructure and Properties of Well-Ordered Multiferroic Pb(Zr,Ti)O₃/CoFe₂O₄ Nanocomposites. *ACS Nano* **4**, 1099–1107 (2010).
- Lukashev, P. V. *et al.* Ferroelectric Control of Magnetocrystalline Anisotropy at Cobalt/Poly(vinylidene fluoride) Interfaces. *ACS Nano* **6**, 9745–9750 (2012).
- Zheng, H. *et al.* Multiferroic BaTiO₃-CoFe₂O₄ nanostructures. *Science* **303**, 661–663 (2004).
- Sahoo, S. *et al.* Ferroelectric control of magnetism in BaTiO₃/Fe heterostructures via interface strain coupling. *Phys. Rev. B* **76**, 092108 (2007).
- Fechner, M. *et al.* Magnetic phase transition in two-phase multiferroics predicted from first principles. *Phys. Rev. B* **78**, 212406 (2008).
- Picozzi, S., Yamauchi, K. & Sanyal, B. Interface effects at a half-metal/ferroelectric junction. *Appl. Phys. Lett.* **91**, 062506 (2007).
- Weisheit, M. *et al.* Electric field-induced modification of magnetism in thin-film ferromagnets. *Science* **315**, 349–351 (2007).
- Duan, C.-G. *et al.* Surface magnetoelectric effect in ferromagnetic metal films. *Phys. Rev. Lett.* **101**, 137201 (2008).
- Nakamura, K. *et al.* Giant Modification of the Magnetocrystalline Anisotropy in Transition-Metal Monolayers by an External Electric Field. *Phys. Rev. Lett.* **102**, 187201 (2009).
- Zhang, S. Spin-Dependent Surface Screening in Ferromagnets and Magnetic Tunnel Junctions. *Phys. Rev. Lett.* **83**, 640 (1999).
- Niranjan, M. K., Velev, J. P., Duan, C. G., Jaswal, S. S. & Tsymbal, E. Y. Magnetoelectric effect at the Fe₃O₄/BaTiO₃ (001) interface: A first-principles study. *Phys. Rev. B* **78**, 104405 (2008).
- Fechner, M., Ostanin, S. & Mertig, I. Effect of oxidation of the ultrathin Fe electrode material on the strength of magnetoelectric coupling in composite multiferroics. *Phys. Rev. B* **80**, 094405 (2009).
- Rondinelli, J. M., Stengel, M. & Spaldin, N. A. Carrier-mediated magnetoelectricity in complex oxide heterostructures. *Nat. Nanotech.* **3**, 46–50 (2008).
- Duan, C.-G. Interface/surface magnetoelectric effects: New routes to the electric field control of magnetism. *Front. Phys.* **7**, 375–379 (2012).
- Burton, J. D. & Tsymbal, E. Y. Prediction of electrically induced magnetic reconstruction at the manganite/ferroelectric interface. *Phys. Rev. B* **80**, 174406 (2009).



29. Vaz, C. A. F. *et al.* Origin of the Magnetoelectric Coupling Effect in $\text{Pb}(\text{Zr}_{0.2}\text{Ti}_{0.8})\text{O}_3/\text{La}_{0.8}\text{Sr}_{0.2}\text{MnO}_3$ Multiferroic Heterostructures. *Phys. Rev. Lett.* **104**, 127202 (2010).
30. Ding, H.-C. & Duan, C.-G. Electric-field control of magnetic ordering in the tetragonal-like BiFeO_3 . *Europhys. Lett.* **97**, 57007 (2012).
31. Laukhin, V. *et al.* Electric-field control of exchange bias in multiferroic epitaxial heterostructures. *Phys. Rev. Lett.* **97**, 227201 (2006).
32. Chu, Y.-H. *et al.* Electric-field control of local ferromagnetism using a magnetoelectric multiferroic. *Nat. Mater.* **7**, 478–482 (2008).
33. Bihlmayer, G., Koroteev, Y. M., Echenique, P. M., Chulkov, E. V. & Blügel, S. The Rashba-effect at metallic surfaces. *Surf. Sci.* **600**, 3888–3891 (2006).
34. Gong, S.-J., Duan, C.-G., Zhu, Y., Zhu, Z.-Q. & Chu, J.-H. Controlling Rashba spin splitting in $\text{Au}(111)$ surface states through electric field. *Phys. Rev. B* **87**, 035403 (2013).
35. Ohno, H. *et al.* Magnetization vector manipulation by electric fields. *Nature* **455**, 515–518 (2008).
36. Maruyama, T. *et al.* Large voltage-induced magnetic anisotropy change in a few atomic layers of iron. *Nat. Nanotech.* **4**, 158–161 (2009).
37. Tsujikawa, M. & Oda, T. Finite Electric Field Effects in the Large Perpendicular Magnetic Anisotropy Surface $\text{Pt}/\text{Fe}/\text{Pt}(001)$: A First-Principles Study. *Phys. Rev. Lett.* **102**, 247203 (2009).
38. Tsymbal, E. Y. Spintronics: Electric toggling of magnets. *Nat. Mater.* **11**, 12–13 (2012).
39. Velev, J. P., Jaswal, S. S. & Tsymbal, E. Y. Multi-ferroic and magnetoelectric materials and interfaces. *Phil. Trans. Royal Soc. A* **369**, 3069–3097 (2011).
40. Wang, W.-G., Li, M., Hageman, S. & Chien, C. L. Electric-field-assisted switching in magnetic tunnel junctions. *Nat. Mater.* **11**, 64–68 (2012).
41. Shiota, Y. *et al.* Induction of coherent magnetization switching in a few atomic layers of FeCo using voltage pulses. *Nat. Mater.* **11**, 39–43 (2012).
42. Kanai, S. *et al.* In-plane magnetic field dependence of electric field-induced magnetization switching. *Appl. Phys. Lett.* **103**, 072408 (2013).
43. Bauer, U., Przybylski, M., Kirschner, J. & Beach, G. S. D. Magnetoelectric Charge Trap Memory. *Nano Lett.* **12**, 1437–1442 (2012).
44. Zhu, W. J., Liu, Y. W. & Duan, C.-G. Modeling of the spin-transfer torque switching in FePt/MgO -based perpendicular magnetic tunnel junctions: A combined ab initio and micromagnetic simulation study. *Appl. Phys. Lett.* **99**, 032508 (2011).
45. Honolka, J. *et al.* Magnetism of FePt Surface Alloys. *Phys. Rev. Lett.* **102**, 067207 (2009).
46. Niranjana, M. K., Duan, C.-G., Jaswal, S. S. & Tsymbal, E. Y. Electric field effect on magnetization at the $\text{Fe}/\text{MgO}(001)$ interface. *Appl. Phys. Lett.* **96**, 222504 (2010).
47. Kresse, G. & Furthmüller, J. Efficient iterative schemes for ab initio total-energy calculations using a plane-wave basis set. *Phys. Rev. B* **54**, 11169 (1996).
48. Neugebauer, J. & Scheffler, M. Adsorbate-substrate and adsorbate-adsorbate interactions of Na and K adlayers on $\text{Al}(111)$. *Phys. Rev. B* **46**, 16067 (1992).
49. Daalderop, G. H. O., Kelly, P. J. & Schuurmans, M. F. H. First-principles calculation of the magnetocrystalline anisotropy energy of iron, cobalt, and nickel. *Phys. Rev. B* **41**, 11919 (1990).
50. Zhang, H., Hou, Z., Zhang, J., Zhang, Z. & Liu, Y. Precession frequency and fast switching dependence on the in-plane and out-of-plane dual spin-torque polarizers. *Appl. Phys. Lett.* **100**, 142409 (2012).

Acknowledgments

This work was supported by the National Key Project for Basic Research of China (Grants No. 2013CB922301, 2014CB921104), NSFC (Grant Nos. 61125403, 11004211 and 11274241), Program of Shanghai Subject Chief Scientist. Computations were performed at the ECNU computing center.

Author contributions

C.G.D. conceived and designed this project and analyzed the results in the first-principles calculation. Y.L. was involved in explaining the data from the LLG-based simulation. D.X. modified the simulation program and did some calculation work for supplementary results. W.Z. and S.J.G. carried out the first-principles and simulating calculations and wrote the paper. All the authors reviewed and modified the manuscript.

Additional information

Competing financial interests: The authors declare no competing financial interests.

How to cite this article: Zhu, W.J., Xiao, D., Liu, Y.W., Gong, S.J. & Duan, C.-G. Picosecond electric field pulse induced coherent magnetic switching in $\text{MgO}/\text{FePt}/\text{Pt}(001)$ -based tunnel junctions: a multiscale study. *Sci. Rep.* **4**, 4117; DOI:10.1038/srep04117 (2014).



This work is licensed under a Creative Commons Attribution-NonCommercial-ShareAlike 3.0 Unported license. To view a copy of this license, visit <http://creativecommons.org/licenses/by-nc-sa/3.0>